Improved Modelling for Vertical Profiles of Flow Speed in a Turbulent Tidal Channel

Lilli F. Enders, Richard H. Karsten, Maricarmen Guerra, Alex E. Hay

Abstract—**The Minas Passage, one of the Bay of Fundy's tidal channels, located in Nova Scotia, Canada, presents significant potential for tidal energy development because of its highly energetic flows. Tidal energy deployments in Minas Passage have historically been bottom-mounted and stationary, and the potential transition to arrays of floating turbines requires additional considerations. Particularly, this new application demands characterization of flow over the entire water column, including near the free surface. Observational site characterization efforts in Minas Passage have primarily consisted of stationary, bottom mounted Acoustic Doppler Current Profiler (ADCP) deployments. Using ADCP records collected in Minas Passage, we fit the vertical profiles of velocity using three methods: logarithmic law of the wall, power law, and an adapted logarithmic law of the wall which includes a "wake function" to improve fits in the upper water column. We find that although the law of the wall results in well-fitted estimations of the vertical velocity profiles near the seabed ($z < 10m$), observational profiles consistently deviate from the fitted curves in the middle and upper water column, recording significantly faster flow speeds than predicted by the law of the wall. The adapted model, which is rooted in turbulence theory and includes a wake term, is successful in capturing flow in the outer layer of the water column and allows for reverse shear to be captured in the profile. The resulting fits show a sizeable reduction in error throughout the entirety of the water column compared to the law of the wall profiles, and consistently reduce the error in the vertical profile fits when compared to power law fits. In addition to resulting in low error for both individual and averaged vertical profiles of flow, the physical quantities estimated from the adapted model, including the bottom drag coefficient, agree well with those computed from the law of the wall, demonstrating the physical usefulness of the adapted model.**

Keywords—**vertical profiles, power law, law of the wake, ADCP, tidal flow.**

I. Introduction

The high-energy flow at potential tidal energy sites generates turbulent boundary layers that extend from the seafloor to the surface. Understanding and characterizing the vertical profiles of the flow in the boundary layer is important for optimizing turbine performance, improving flow modelling, and extrapolating mid-depth observations to the surface. Most previous studies, for example [1] and [2], have focused on applying the power law for this purpose. Other works (such as that by Milne et al. [3]) have used the "law of the wake" first introduced by Coles [4]. Here we examine the vertical profiles of ADCP data from a tidal site in the Minas Passage. We compare the two approaches, examining both time means over long-time means (full tidal cycles and deployments), and individual 5-minute ensembles. We compare each method to the well-established law of the wall as a baseline.

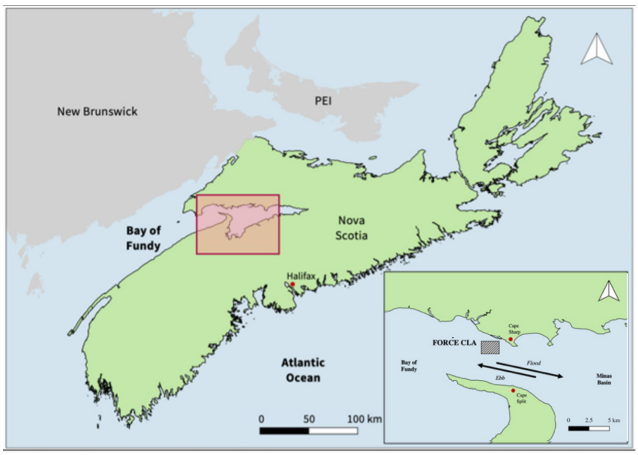

Fig. 1 The Bay of Fundy, showing the location of Minas Passage, red box. The inset shows Minas Passage, the location of the FORCE CLA, and the direction of the flood and ebb tides.

 This work was supported in part by a MITACS internship in partnership with FORCE.

L. F. Enders is with the Department of Earth and Planetary Sciences at Massachusetts Institute of Technology, Cambridge, Massachusetts, United States (e-mail: lenders@mit.edu).

R. H. Karsten is with the Department of Mathematics and Statistics, Acadia University, Wolfville, Nova Scotia, Canada. (e-mail: richard.karsten@acadiau.ca).

M. Guerra is with the Department of Civil Engineering at Universidad de Concepción and with Center for Oceanographic Research COPAS COASTAL, Barrio Universitario s/n, Concepcion, Chile (e- mail: marguerra@udec.cl).

A. E. Hay is with the Department of Oceanography, Dalhousie University, Halifax, Nova Scotia, Canada (e-mail: alex.hay@dal.ca).

Digital Object Identifier: https://doi.org/10.36688/ewtec-2023-563

A. *Previous Studies*

Determining the form of the mean vertical profile of turbulent flow has a long history. The derivations of the "law of the wall" and the "power law" go back to the work of von Kármán [5] and Prandtl [6]. There has been considerable discussion about whether the laws are "universal" or dependent on Reynolds number, and whether the laws can be rigorously derived or established empirically (see for example [7], which argues strongly against the "universal logarithmic law" and for the "nonuniversal power law").

The law of the wall, see Equation (1), can be derived using similarity arguments, see for example [8]. It is often used to describe the velocity near the bottom, in what is called the logarithmic boundary layer. The law of the wall has been shown to accurately model the bottom boundary layer in tidal flows [9][10], but it generally does not extend through the entire water column. For bottom mounted ADCP data, the law of the wall is usually fit only to measurements near the sea bottom. The depth for which the law of the wall applies is usually determined by keeping the error of the fit below some maximum value [9] [10][11].

The "power law" can also be derived through similar arguments [7] or from a balance of advection and viscous terms, as shown by de Chant [12]. Although the law is sometimes referred to as the 1/7th law, it has been argued that the value of the exponent varies with Reynolds number [5][7][12]. While the power law satisfies the no-slip condition at the bottom, it is often thought that the "validity of this power formula ceases in the immediate neighborhood of the wall."[5] In terms of recent application of the power law to tidal flows, Lewis et al. [1] examined the vertical profiles of two ADCPs in the Irish Sea, deployed 47.5 and 28.6 days in water depths of 33.5 m and 86.6 m, respectively. The profiles were 1-hour means with a depth-averaged velocities greater than 1 m/s. Or more recently, Sentchev et al. [2] examined the vertical profiles from a single ADCP in Alderney Race deployed for 15 days in a water depth of 33.5 m The profiles were 1-hour means, 10 profiles for each tidal cycle centered on the peak flow.

There is also a less-known model introduced by Coles [4]: the "law of the wake," see Equation (4). For simplicity we will refer to this as the "wake law." Coles showed that the velocity deficit outside the boundary layer had a consistent form that could be described by a "wake" function, since the dynamics in this layer were similar to that of a wake. As such, the wake law can be seen as an extension of the law of the wall beyond the logarithmic boundary layer, to the entire water column. More recently, the wake law has been discussed by Schultz and Flack [13] and a number of works by Guo and collaborators [14][15][16][17]. In terms of recent application to tidal flows, Milne et al. [3] examined the vertical profile of ADCP data deployed in Pentland Firth, using data 2 hours either side of the peak flow from the three consecutive ebb tides. They compared the profiles to the law of the wall and wake, using a friction velocity calculated using the Reynolds stress and a constant wake amplitude.

B. *Site Description*

The Minas Passage (see Fig. 1), one of the Bay of Fundy's tidal channels, presents significant potential for tidal energy development because of its highly energetic flows [18]. Flow in Minas Passage routinely exceeds 5 m/s and is highly turbulent ($Re \approx 10^8$) [11]. The Fundy Ocean Research Centre for Energy (FORCE) has established berths for testing tidal turbines within a Crown Lease Area (CLA), see [19]. The CLA is in the northern portion of the Minas Passage (Fig. 1 inset) and has water depths varying from 30 to 60 m, see (Fig. 2). Although great strides have been made towards the complete characterization of the water column in Minas Passage and at similar sites in Nova Scotia, some aspects of the flow are yet to be explored in depth. In particular, the characterization of vertical profiles extending through the entirety of the water column have not been derived for Minas Passage.

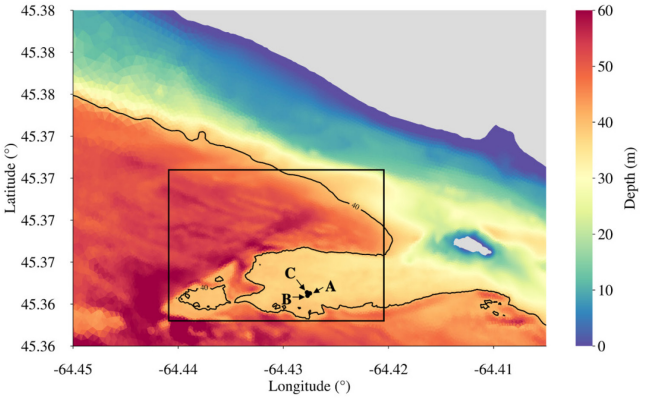

Fig. 2 The location of the three ADCPs (black dots) in the FORCE CLA (rectangle). The colours show the mean water depth. The black contour has a depth of 40 m.

C. *ADCP Data*

The current velocity data considered here are derived from three Acoustic Doppler current profiler (ADCP) deployments in Minas Passage, Bay of Fundy (*Fig. 2.*) The deployments were part of a project led by Acadia University and FORCE to quantify the capabilities of acoustic devices to derive spatiotemporal distributions of fish species [20]. A single five-beam Nortek Signature 500 kHz ADCP was deployed three times on a stationary platform called 'FAST-3'. *Table 2* lists the details of the three deployments, including the number of ensemble-mean vertical profiles used in the analysis.

For all deployments, the ADCP was set to record continuously (in burst mode) for 5 minutes every 15 minutes with all five of its beams. ADCPs A and C recorded at 4 Hz, the maximum sampling frequency for continuous recording using all five beams. ADCP B recorded with a sampling frequency of 2 Hz. For each deployment, the ADCP recorded averaged raw data in one-metre vertical cells, with the bottom cell beginning at 0.5 m above the seabed (to account for the height of the platform and blanking distance) and ending at 1.5 m above

the seabed, and the top cell extending 49 m from the ADCP to capture the maximum water depths at the site. In each instance, the instrument platform was deployed within 25 m of the other deployments. The ADCPs were deployed on a volcanic platform that stretches from a small island (Black rock) across the southern portion of the FORCE CLA. The volcanic platform is relatively flat with a mean water depth between 35 to 40m. The surrounding water is much deeper, 50 to 60 m, where the sea bottom is much rougher. The abrupt edge of the platform is roughly 450 m upstream on the flood tide and 200 m upstream on the ebb tide.

Table 1 ADCP properties

ADCP	*Start Date*	*Days*	*Depth*	*Profiles*
A	2017-12-14	65	38 m	4749
B	2018-03-30	53	36 m	3739
C	2018-09-15	74	38 m	5352

D. Paper Summary

In this work, we examine the vertical profiles of the flow from the three ADCP deployments discussed above. We examine both short (5 min) and long-time (4-6 hour) means of the data. We focus on the entire water column, comparing the power law to the law of the wake in terms of the quality of fit and the variation in the parameter values.

II. Methods

E. Normalizing ADCP data

We begin by describing the normalization of the ADCP data. Fig. 3 shows the signed speed for 3 days of data from ADCP A during a spring tide. The tidal range has a maximum value of 13.5 m over this time frame. The signed speed ranges from -3.9 to 5.3 m/s, with positive values denoting flow during flood tides, and negative values denoting flow during ebb tides. Flood speeds are on average 1.25 times larger than ebb. A height of 85% of the total water column was used as a threshold for removal of data contaminated by sidelobe reflections from the surface. Data above this threshold were removed (see [11] for details).

Since the tidal range at the site is so large, it is useful to use a scaled vertical variable, $\eta = z/h$, where h is the mean water depth for the ensemble, so that $0 \le \eta \le 1$. The ADCP data is interpolated onto 38 levels running from $\eta = 0.035$ to $\eta = 0.985$ with $\Delta\eta = 0.025$, which approximately equal to the 1 m ADCP bin size. The lowest value of $\eta = 0.035$ is chosen so that it is above the lowest bin for all ADCP ensembles. The middle plot in Fig. 3 shows the speeds versus the normalized coordinate η. The use of a normalized vertical coordinate is standard in the analysis of turbulent boundary layers, but the choice of vertical coordinate can vary depending on whether the focus is the inner or outer boundary layer (see for example [13])

Finally, to concentrate on the vertical profile variation and allow for informative averaging of different profiles from different ensembles, we normalize the speeds by the depth averaged speed at each time. The result is shown in the bottom plot of Fig. 3. We only consider the non-slack flow, when ebb speeds exceed 1.25 m/s and flood speeds exceed 1.5 m/s (the results are not sensitive to these choices). Approximately 75% of all the ensembles meet this criterion. The result is show in the bottom plot of Fig. 3.

Through this normalization process, nearly all indications of the tidal cycle have been removed. While there are still variations in the normalized speed with time, these variations are significantly smaller than the vertical variations and do not have a regular pattern in time. It is therefore reasonable to think that the vertical profiles can be represented by simple functions that vary little over time.

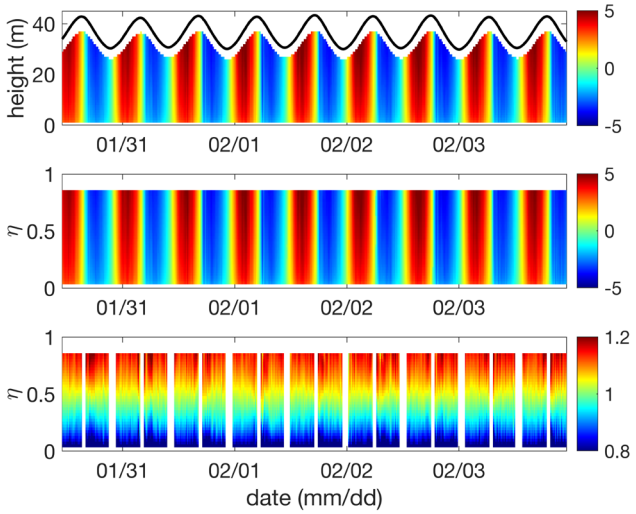

Fig. 3 Data from ADCP A for 3 days in 2018. Top, signed speed (m/s) vs height above the bottom; middle, signed speed (m/s) vs $\eta = z/h$; bottom, speed normalized by the depth average speed vs η.

III. Models of the Vertical Profiles

We now examine the forms of the vertical profile models. We write the law of the wall as

$$u(\eta) = \frac{u_*}{\kappa}[\,\ln(\eta) + B\,], \quad (1)$$

where u_* is the friction velocity, $\kappa = 0.41$ is the von Kármán constant and B is a constant that can be related to the bottom roughness length scale. It is useful to interpret the friction velocity in terms of a bottom drag,

$$C_D = \left(\frac{u_*}{U}\right)^2, \quad (2)$$

where U is a reference velocity, here chosen to be the depth averaged velocity.

The power law can be written as

$$u(\eta) = \left(\frac{\eta}{\beta}\right)^{\frac{1}{\alpha}} = U_s\, \eta^{\frac{1}{\alpha}} \quad (3)$$

where α is the power/exponent. The parameter β in (3) is a measure of roughness but, as (3) shows, the equation can also be rewritten to interpret it as the surface velocity, $U_s = u(1)$.

Finally, the law of the wake is formed by adding a wake function to the law of the wall:

$$u(\eta) = \frac{u_*}{\kappa}[\,\ln(\eta) + B + \Pi\, w(\eta)] \quad (4)$$

where $w(\eta)$ is the wake function and Π is the amplitude of the wake function. (Note that there are a variety of notations used to write the law of the wake, see for example [13].) The wake function has been chosen in previous studies to have many forms, but most often is chosen to satisfy the following conditions:

$$w(0) = w'(0) = w'(1) = 0, w(1) = 1. \quad (5)$$

Here we choose the cubic wake function, following [3]:

$$w(\eta) = \eta^2(3 - 2\eta). \quad (6)$$

Other possibilities are a sinusoidal function or a Sine integral function (see [13],[14],[15],[16]), which have nearly the identical shape over the range $0 \le \eta \le 1$. This choice does not significantly affect the results.

The parameters foreach model are fit to the ADCP data using MATLAB's fminsearch function to minimize the sum of the squared error. For the law of the wall, the curve was fit to only the bottom 6 data points. For the law of the wake and power law, the model is fit to all data between $\eta = 0.05$ and $\eta = 0.8$. This range was chosen to guarantee quality data for all ensembles for all ADCPs.

IV. Results

F. Law of the wall

Enders [11] examined the law of the wall for ADCP A in detail and found that that the model fit the data accurately up to heights of 5 to 8m above the seabed with the fitted curve exhibiting a consistent departure from the measured data at heights greater than 10 m above the seabed. This is clearly shown in Fig. 4, where the law of the wall curve is accurate for the bottom 20% of the profile but not for the upper 50% of the profile. The conclusion is clear, the law of the wall was not suitable for the entire vertical profile. Below, we compare the calculation of bottom drag using (2) for the wall of the law fit to the wake law fit.

G. Mean Flood and Ebb Profiles

Vertical profiles are often considered for long-time averages of turbulent flow. So, we first consider the averages of all ebb and flood ensembles for each ADCP. An example result for all flood tides for ADCP A is shown in Fig. 4. Here we show the mean ADCP velocity, with errors bars of ± 1 standard deviation (It should be noted that the variation in the ADCP data over the more than 2000 ensembles as indicated by the error bars in Fig. 4, is quite small. The maximum coefficient of deviation (SD/mean) is only 3%).

Curves of best fit are also plotted for the law of the wall, law of the wake and power law (Fig. 4). Errors are given in Table 2 and parameter values in Fig. 4. The figure shows that the speed exceeds that predicted by the law of the wall. The power law fits the data well, with errors less than the standard deviation of the ADCP data, and a root mean square error (RMSE) of 0.95%. (Note that since all profiles are normalized by the depth averaged flow, the RMSE can be expressed as a percentage error.) The law of the wake is an almost perfect fit, with an RMSE only 0.12%. This quality of fit is consistent for the ebb tide and for the other two ADCPs (see Table 2). Note, the parameter values for the curves in Fig. 4 appear as the outlined red squares in the plots below.)

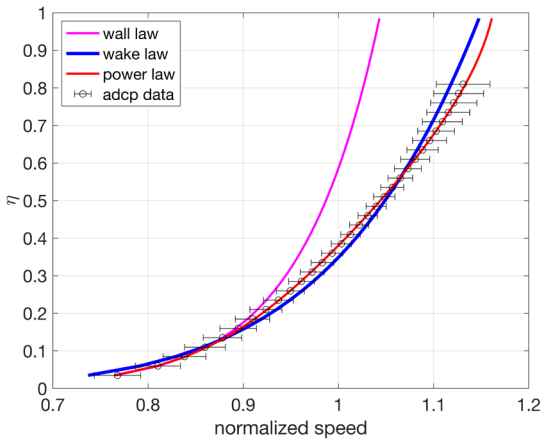

Fig. 4 Result of fitting the law of the wall, law of the wake and power law functions to the normalized flood data from ADCP 1

H. Ensemble Profiles RMSEs

We next examine fitting curves to each individual ensemble. The RMSE for these fits are shown in Table 2. As one would expect, the RMSE for the wake law are smaller than the power law with a smaller SD Their errors show little variation between ebb and flood within or between the three ADCPs.

To demonstrate the range of errors more clearly over all the ensembles, we plot the cumulative distribution function (cdf) in Fig. 5. Remarkably, it shows that for the wake law over 75% of the ensembles have an RMSE of less than 1%. For the parameter discussion below, we consider an RMSE < 1.35% to be a good fit, covering 87% of the ensembles. For the power law, only 35% of the ensembles have an RMSE < 1% and to get 87% of the ensembles the good fit criterion must be increased to an RMSE of 2.15%.

(Note, these values are considerably smaller than the SD of the ensemble averages.)

Table 2 The RMSE (%) for the profile curve fits as a percentage. Errors are one standard deviation.

ADCP		Wake Law		Power Law	
		Flood	Ebb	Flood	Ebb
A	Mean	0.14	0.17	1.1	1.0
	Ensembles	0.65±0.31	0.8±0.45	1.35±0.62	1.43±0.65
B	Mean	0.12	0.23	0.75	0.74
	Ensembles	1.0±0.69	0.96±0.65	1.45±0.78	1.40±0.82
C	Mean	0.15	0.26	1.1	0.44
	Ensembles	0.81±0.36	0.91±0.48	1.45±0.57	1.30±0.66

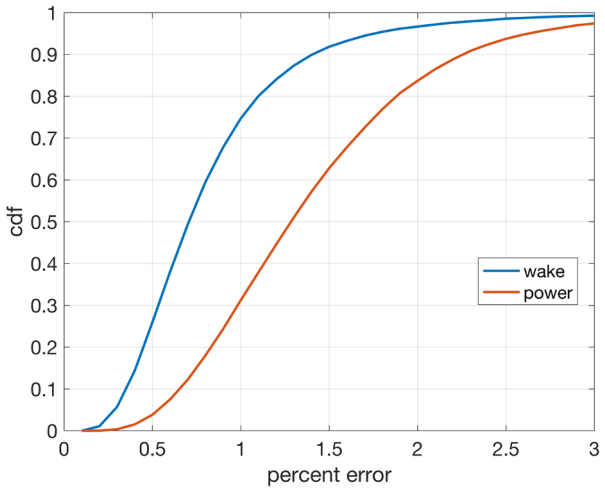

Fig. 5 Comparison of the cumulative distribution function of the ensemble fit RMSEs (%) for the wake and power law fits.

I. Parameter Values

In Fig. 6, we plot the two parameters of the power law fit, α and β, for all ensembles that had an RMSE less than 2.15%, which is 87% of all non-slack ensembles. We see that the mean value of α varies from 5.5 to over 7.8, with standard deviation of 0.81 to 1.16. Combining all ensembles yields a mean value of 6.58±1.20, with a full range of values from 3.0 to 16.0.

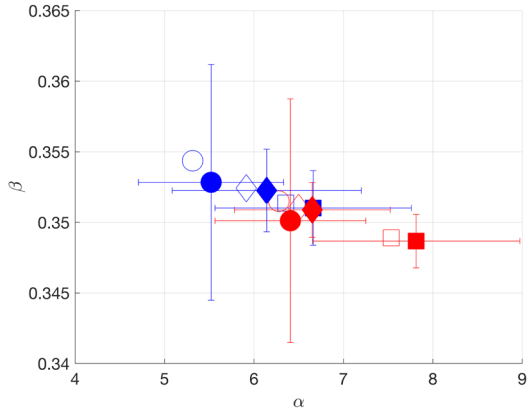

Fig. 6 Values of α and β for power law curve fitting. Red is flood, blue is ebb. Symbols represent the three different ADCPs. Solid symbols are ensemble fits with ± 1 SD error bars, open symbols are for the mean profiles.

The values of α are higher on flood for all 3 ADCPs, but the difference between ebb and flood is within one standard deviation. As the ensemble fits gives values of α slightly larger than the value found from the mean profiles. But the general conclusion is that the variation over a given ensemble, across the different ADCPs, and over flood and ebb is of similar scale, with most falling within ± 1 SD.

The values for α are similar to previous results. Sentchev et al. [21] found values ranging from 5 to 10.8 over all ensembles; the values ranged from 6.4 to 8 when limited to the best fits, RMSE ~ 1%. Lewis et al. [1] found a range of values from 4 to 14, with mean values of 7.1±1.2 and 7.1±2.2. Sentchev et al. [2] found that values of α tended to increase during the tidal cycle. Lewis et al. [1] examined the power coefficient distributions in more detail and did find that the distributions of α were different during different phases of the tide, although not with a clear trend over the two locations. However, it should be noted that Naberezhnykh et al. [22] found α values of 5 or 6 the ebb and flood profiles for two ADCPs also located in the FORCE CLA in similar water depths. The methods used were different than those described here, and the differences need to be examined further.

Lewis et al. [1] examined the power coefficient distributions in more detail and did find that the distributions of α were different during different phases of the tide, although this results was not consistent over the two locations they examined. We have examined the values but have not found a significant difference over the phases of the tides, see the Appendix.

In terms of the roughness parameter, β, we see in Fig. 6 that the value varies over a small range 0.349 to 0.354. Over all ensembles, the mean is 0.351 ± 0.005 and the range is from 0.25 to 0.358, but the lower value is determined by just a few outliers. Lewis et al. [1] also found that the value of the roughness showed a similar small range of variability. They calculated a value of 0.4 ± 0.03, with a range of values 0.3 to 0.5.

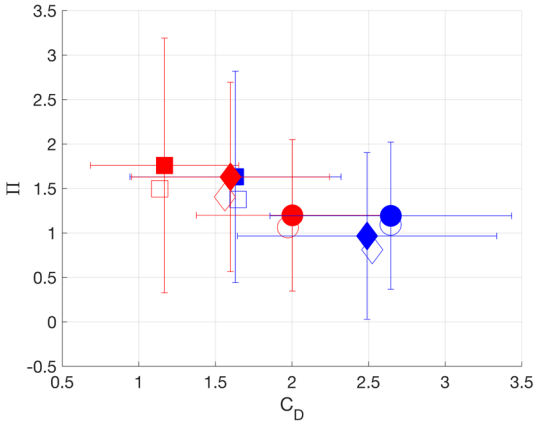

Fig. 7 Values of Π and $C_D(10^{-3})$ for wake law curve fitting. Red is flood, blue is ebb. Symbols represent the three different ADCPs. Solid symbols are ensemble fits with ± 1 SD error bars, open symbols are for the mean profiles.

In Fig. 7 we plot the values of the wake law parameters Π and C_D averaged over all flood and ebb for all ensembles that had an RMSE less than 1.35%, which is 87% of all non-slack ensembles We also compare the mean flood and ebb profiles.

The mean values of Π in Fig. 7 vary from 0.97 to 1.76, with SD of 0.83 to 1.43. The overall mean value is 1.42 ± 1.13. The variation in the means is smaller than the SD, that is, the difference is statistically insignificant. The value are considerably higher than the canonical value of 0.55 used in [3] and found in Coles' original work [23].

Since $w(\eta)$ in (6) is a positive definite function of η, a positive value Π indicates that the wake function increases the flow speed above the law of the wall values, that is faster than a logarithmic fit. The values of Π are positive for 95% of all ensembles. That is, for most of the ensemble profiles, the flow speed is faster than the law of the wall would estimate.

The law of the wake does allow for profiles with reverse shear, $\frac{du}{d\eta} < 0$, if $\Pi < -9/8$. Only 13 of the 12,292 ensembles satisfied this condition, and only 2 of those were fits with a low error. This is not to say that there are no ensembles with reverse shear. The form of the wake law used here restricts the potential of modelling reverse shear. See the Discussion below for other models better suited to modelling reverse shear.

For the bottom drag, C_D, the mean values range from $1.17 - 2.64\ x\ 10^{-3}$ and the SD range from $0.48 - 0.85\ x\ 10^{-3}$. Therefore, there is a considerable range of values centred on the overall mean $1.87\ x\ 10^{-3} \pm 0.86\ x\ 10^{-3}$. The values on ebb are larger than the values on flood, but the difference exceeds 1 SD for one only ADCP. The range of observed C_D values align well with the typical drag coefficient value ($C_D = 2.5\ x\ 10^{-3}$) used in numerical models of the site. Using the law of the wall, Lueck and Lu [9] found values of C_D of $3.5\ x\ 10^{-3} \pm 0.4\ x\ 10^{-3}$ on ebb and $4.0\ x\ 10^{-3} \pm 0.6\ x\ 10^{-3}$ on flood.

It is worthwhile to compare the values of the bottom drag for the wake law to those that are calculated if we only fit the law of the wall to the bottom 6 points of the profile. In Fig. 8, we plot the values of means of $C_D$calculated using these two methods. We see that the means and SD agree extremely well.

However, Fig. 8 is somewhat misleading. If we compare the values for individual ensemble profiles, we find that the individual values do not agree as well. The normalized root mean square difference is 25% and the R^2 value is only 0.48. The conclusion is that the value of the friction velocity and, hence, the bottom drag are sensitive to fitting process. When fitting the wake law to the entire profile, the fit to the logarithmic layer though good is not as accurate as that achieved with the law of the wall. Though the difference in fit is small, because of the logarithmic form of the model, as $\eta \to 0$ the differences in the values of fitted friction velocity can be large.

One reason for fitting a model is to extrapolate the ADCP data to the surface. In Fig. 9 we plot the predicted surface speed for both the wake and power laws. We conclude that both methods will give very similar extrapolated surface speeds. Here the normalized root mean square difference is only 1% and the R^2 value is 0.85.

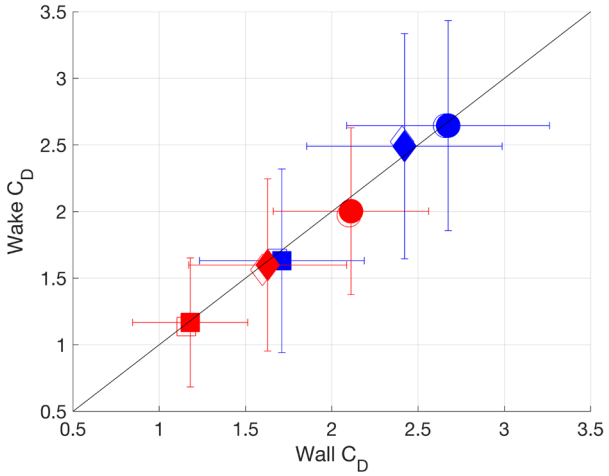

Fig. 8 Values of C_D ($x\ 10^3$)for the wall and wake laws. Colours and symbols as above. The error bars represent one standard deviation, and the black line is when the values are equal. The 1:1 line is indicated in black.

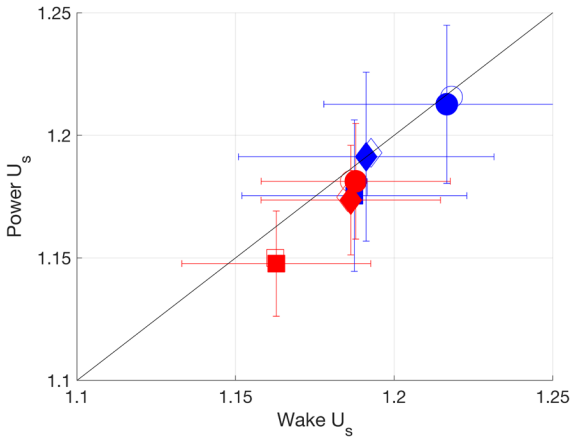

Fig. 9 Values of U_s for the wake and power laws. Colours and symbols as above. The error bars represent one standard deviation, and the black line is when the values are equal.

V. Discussion

The results above illustrate a few key points about the vertical profiles of the flow at this Minas Passage site. The normalization of the data removed the tidal-cycle signal from the results. The normalization is a critical part of the analysis, allowing the vertical profiles at different times to be directly compared and averaged. The fact that both the power law and the wake law capture the profiles with such small RMSE for most of the ensembles is evidence that the flow in Minas Passage is a boundary layer flow, with little influence from surface forcing.

The wake law does capture vertical profiles with a lower RMSE than the power law, almost always within the SD of the measurements. The wake law also does a better job of

representing the near bottom flow, calculates the friction velocity and allows for the calculation of the bottom drag. However, this comes at the cost of fitting an additional parameter.

The fitted parameter values for the power and wake laws found here have similar properties to other studies. The parameter variations over the individual ensembles are larger than the variations between the flood ebb tides and the different ADCPs. One can infer that the vertical profiles are more sensitive to short time variations, likely from the turbulence, than the larger-scale tidal cycle or local spatial variations.

One question that arises from the results is whether one can infer that the 3D flow in Minas Passage can be modelled accurately with a 2D, depth-averaged numerical model plus vertical profile curve. The excellent fit of the power and wake laws suggests yes; the variation of the parameters over the different ensembles suggests no. As a measure of the accuracy of a depth-averaged model, we calculated the RMSE of representing each ensemble profile with the power and wake laws using parameters fit to the flood and ebb averaged data for each ADCP. The results are given in Table 3. All the mean errors are small, < 2.3%, while the SD indicate that there is a larger spread of errors compared to the model fits. For individual ensembles, the error can exceed 15%, but the number of these are small. Approximately 87% of the ensembles have a RMSE less than 3%. The two models give very similar results, indicating that this is a measure of the variation of the normalized vertical profiles, rather than a test of the model fits. And, as shown in Fig. 3 and Fig. 4, this variation is small, roughly 3%.

Table 3. RMSE for 'depth-averaged' model

ADCP		Wake Law		Power Law	
		Flood	Ebb	Flood	Ebb
A	Ensembles	1.6±0.83	2.0±1.1	1.9±0.82	2.3±1.1
B	Ensembles	1.8±1.0	2.1±1.4	1.9±0.96	2.2±1.4
C	Ensembles	1.6±0.8	2.2±1.3	1.9±0.77	2.2±1.3

J. Roughness and Drag

The above results illustrated that the calculated bottom drag coefficient, C_D, showed an asymmetry between flood and ebb tides. This asymmetry might result from the site location, being closer to the edge of the volcanic platform on ebb than flood, resulting in higher 'bottom drag' on ebb compared to flood. But the fact that the drag varied considerably over the ensembles suggests that the bottom drag calculated from vertical profiles is tied more to the turbulent dynamics of the flow than local sea bottom roughness.

One reaches a similar conclusion if one uses the law of the wall or wake law to calculate a roughness scale. The law of the wall/wake are often used to discuss the roughness scales (see [13], [3]). Equation (4) can be rewritten as

$$u(\eta) = \frac{u_*}{\kappa}\left[\ln\left(\frac{z}{k_s}\right) + \Pi\, w(\eta)\right], \tag{7}$$

where $k_s = h\exp(-B)$ is a roughness scale measured in meters. (Note the definition of the roughness scale will vary depending on how the vertical variable is normalized). If we calculate the roughness scale using the ensemble data, we find a mean value of $log_{10}(k_s) = -3.2 \pm 1.1$, that is, the values range over more than four orders of magnitude for 2 standard deviations. These results are similar to other studies using the law of the wall which find roughness estimates that are scattered over at least one order of magnitude [9], [24].

Since the sea bottom is not changing over this time, one can only conclude that the parameter B is not telling us accurate information about the sea bottom. Rather, when fitting to full vertical profiles, the parameter B is being determined more by the depth averaged flow. One possible solution to this problem is to add a parameter to the model representing the zero-plane displacement, as is often done to account for rough topography in atmospheric boundary layer models. However, accurately fitting this additional parameter requires more data from the near bottom boundary layer.

Given that the power law roughness parameter, β, shows little variation over the ensemble fits, one might conclude that the power law is better for modelling the bottom boundary layer. However, it should be emphasized that the power law does not fit the bottom boundary layer nearly as well as the law of the wall and wake law, see Fig. 4. If we examine the normalized RMSE over the bottom 6 points of data, the law of the wall has a mean error of 0.53±0.35%, with over 90% of the profiles with an error of less than 1%. The wake law has a mean error 1.0±0.74% with only 60% of the profiles with an error of less than 1%. And the power law has a mean error 2.0±1.1% with only 20%. This is a significant difference, larger than that for the full profile. It suggests that using the power law to estimate bottom roughness may not be that accurate.

K. Reverse Shear

One purpose of examining the vertical profiles of the flow is to determine if extreme values of the shear occur. When long-time averages of tidal flow are examined, we expect results like those found here, that the profiles can be modelled well by a power or log-layer law, indicating a positive shear throughout the water column that decreases with height above the bottom. The wake law results above agree with this characterization, with a positive wake amplitude indicating that the profiles are faster than a logarithmic law, and thus have a higher positive shear. The form of the wake law used here was chosen for its similarity to the power law.

As discussed above, the wake law can model profiles with reverse shear with large negative values of the wake amplitude. However, this rarely occurs, because the form of the wake law used here (4) enforces a positive shear at the surface, namely:

$$\frac{du}{d\eta} = \frac{u_*}{\kappa} \text{ at } \eta = 1. \quad (8)$$

Note that this is like the power law which gives:

$$\frac{du}{d\eta} = \frac{U_s}{\alpha} \text{ at } \eta = 1. \quad (9)$$

That is, in both cases, the surface conditions are determined by the fit of the law to the entire vertical profile.

For the wake law, it is odd that the surface condition stress condition is determined by the bottom friction velocity. However, the wake law can be modified to meet any surface boundary condition. For example, following Guo and Julien [14], we can rewrite (4) as

$$u(\eta) = \frac{u_*}{\kappa}\left[\ln(\eta) + B + \Pi\, w(\eta) - \frac{\eta^3}{3}\right] \quad (10)$$

so that the equation satisfies a zero-stress boundary condition at the surface, that is,

$$\frac{du}{d\eta} = 0 \text{ at } \eta = 1, \quad (11)$$

We have completed the fitting process using this modified wake law and the results are qualitatively the same, with similar RMSE values and a similar distribution of parameters values. There are two minor changes. First, the conditions lower the predicted surface speed, U_s, by about 10%. Second, by reducing the surface stress, this form of the wake law can fit profiles with reverse shear more readily. While the zero-stress condition might be considered more physical, it still does not allow for cases of extreme shear, nor can it accurately identify profiles where the surface stress is non-zero.

Note that one could adapt (10) to specify any value for the surface stress. Or, following [15], one could redefine the wake function so that the surface stress is an additional parameter to be determined through the fitting process. In practice, this further reduces the RMSE of the curve fits, particularly in cases where the profile is not monotonic. But it also predicts a wide range of surface flow conditions, often with extreme velocities, if used to extrapolate to the surface. In theory, such a model could be used to identify cases where a surface stress through wind or waves is acting on the flow. But without ADCP measurements in the surface boundary layer, we do not have the data to accurately determine this parameter. Furthermore, such a model assumes that reverse shear is related to surface conditions. For this site, this does not appear to be the case, with reverse shear occurring through the water column and during times when no surface stress is apparent. When Enders [11] explored the impact of extreme wind conditions on the ADCP data, they found no evidence that it affected the horizontal flow. Our conclusion is that these more complex profile models are not suitable nor needed for Minas Passage. Examining these more complex profile models at other sites, especially those where wind and waves affect the flow deep into the water column is left for future work.

APPENDIX

In previous works [1][2], the analysis of the flow profiles has included an analysis of how the model parameters change with flow speed and phase of the tide. In our analysis of the Minas Passage site, we did not find these to be important. But for completeness, we include this analysis here in the appendix.

In Fig. 10 we plot the depth-averaged speed of all ensembles versus tide time. Tide time runs from 0 at low tide to 1 at the subsequent low tide with high tide at roughly 0.5. Peak flood occurs at roughly 0.25; peak ebb at 0.75. Means and SD are calculated over bins of size 1/12.5 or roughly 1 hour in time. The figure shows the strong asymmetry between flood and ebb and the rapid acceleration of the ebb tide that results from an eddy passing through the region at the end of the slack.

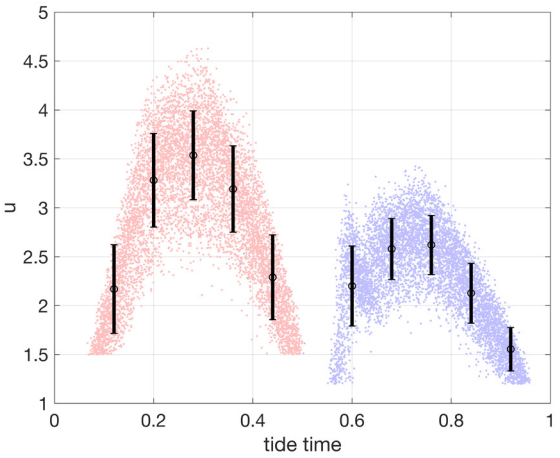

Fig. 10 Ensemble mean velocity versus tide time, red for flood, blue for ebb. The black lines are the averages over a time roughly equivalent to one hour. Error bars are one SD.

In the following figures, Fig. 11 ,Fig. 12 Fig. 13, and Fig. 14, we plot the fit parameters for the law of the power and wake law models for all flood and ebb ensembles for the three ADCPs. The values are plotted vs the depth mean speed of the ensemble, with means and SD calculated for 0.5 m/s speed bins. They are also plotted vs tide time, as described above.

For all the parameters, the variation with flow speed and the variation with tide time is always less than the SD associated with the binned ensembles. , Fig. 11 does show that α tends to have lower values of the ebb tide (centred around 6) than on the flood tide (centred around 7) Fig. 13

also shows that the calculated drag coefficient for the wake law is higher on the ebb than on the flood.

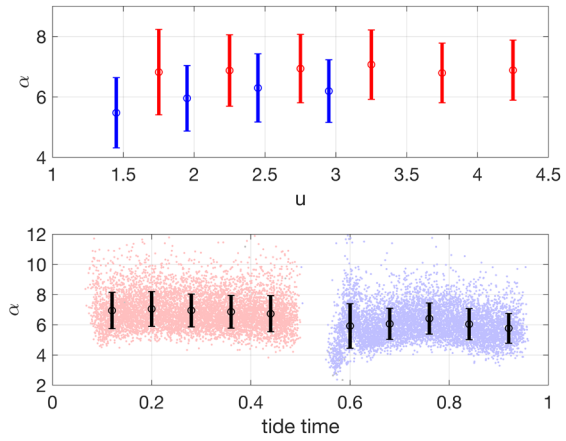

Fig. 11 Variation of α with mean speed (top) and tide time (bottom). Error bars are one sd. All values are shown as dots in the bottom plot, red for flood, blue for ebb.

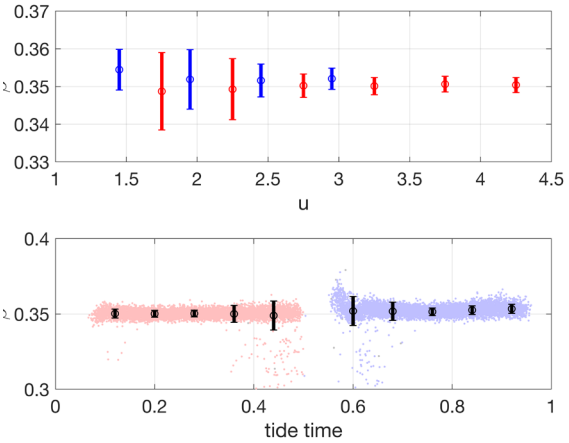

Fig. 12 Variation of β with mean speed (top) and tide time (bottom). Error bars are one sd. All values are shown as dots in the bottom plot, red for flood, blue for ebb.

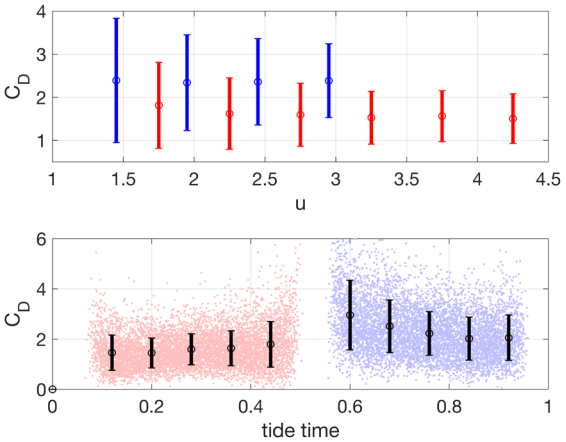

Fig. 13 Variation of C_D with mean speed (top) and tide time (bottom). Error bars are one sd. All values are shown as dots in the bottom plot, red for flood, blue for ebb.

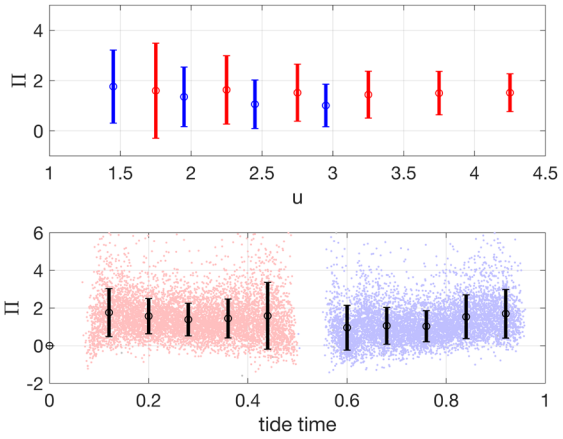

Fig. 14 Variation of Π with mean speed (top) and tide time (bottom). Error bars are one sd. All values are shown as dots in the bottom plot, red for flood, blue for ebb.

ACKNOWLEDGEMENT

Funding and other support for this research was supplied by Mitacs Canada and the Fundy Ocean Research Centre for Energy (FORCE).

[1] M. Lewis, S. P. Neill, P. Robins, M. R. Hashemi, and S. Ward, "Characteristics of the velocity profile at tidal-stream energy sites," *Renew. Energy*, vol. 114, pp. 258–272, Dec. 2017, doi: 10.1016/j.renene.2017.03.096.

[2] A. Sentchev, T. D. Nguyen, L. Furgerot, and P. Bailly du Bois, "Underway velocity measurements in the Alderney Race: towards a three-dimensional representation of tidal motions," *Philos. Trans. R. Soc. A*, vol. 378, no. 2178, p. 20190491, 2020.

[3] I. A. Milne, J. M. R. Graham, and D. S. Coles, "On the scaling of turbulence in a high Reynolds number tidal flow," *J. Fluid Mech.*, vol. 915, p. A104, May 2021, doi: 10.1017/jfm.2021.169.

[4] D. S. Coles, "The law of the wake in the turbulent boundary layer," *J. Fluid Mech.*, vol. 1, no. 2, pp. 191–226, doi: 10.1017/S0022112056000135.

[5] T. Von Kármán, *Mechanical similitude and turbulence*. National Advisory Committee for Aeronautics, 1931.

[6] "20050029454.pdf." Accessed: May 22, 2023. [Online]. Available: https://ntrs.nasa.gov/api/citations/20050029454/downloads/20050029454.pdf

[7] G. I. Barenblatt, A. J. Chorin, and V. M. Prostokishin, "Turbulent flows at very large Reynolds numbers: new lessons learned," *Phys.-Uspekhi*, vol. 57, no. 3, p. 250, Mar. 2014, doi: 10.3367/UFNe.0184.201403d.0265.

[8] S. B. Pope and S. B. Pope, *Turbulent flows*. Cambridge university press, 2000.

[9] R. G. Lueck and Y. Lu, "The logarithmic layer in a tidal channel," *Cont. Shelf Res.*, vol. 17, no. 14, pp. 1785–1801, Dec. 1997, doi: 10.1016/S0278-4343(97)00049-6.

[10] J. M. McMillan, A. E. Hay, R. G. Lueck, and F. Wolk, "Rates of Dissipation of Turbulent Kinetic Energy in a High Reynolds Number Tidal Channel," *J. Atmospheric Ocean. Technol.*, vol. 33, no. 4, pp. 817–837, Apr. 2016, doi: 10.1175/JTECH-D-15-0167.1.

[11] L. Enders, "FLOW CHARACTERIZATION AT A TURBULENT TIDAL ENERGY SITE IN MINAS PASSAGE, BAY OF FUNDY," MSc Thesis, Acadia University, 2022.

[12] L. J. De Chant, "The venerable 1/7th power law turbulent velocity profile: a classical nonlinear boundary value problem solution and its relationship to stochastic processes," *Appl.*

Math. Comput., vol. 161, no. 2, pp. 463–474, Feb. 2005, doi: 10.1016/j.amc.2003.12.109.

[13] M. P. Schultz and K. A. Flack, "The rough-wall turbulent boundary layer from the hydraulically smooth to the fully rough regime," *J. Fluid Mech.*, vol. 580, pp. 381–405, Jun. 2007, doi: 10.1017/S0022112007005502.

[14] J. Guo and P. Y. Julien, "Application of Modified Log-Wake Law in Open-Channels," pp. 1–9, Apr. 2012, doi: 10.1061/40856(200)200.

[15] J. Guo, "Second Log-Wake Law from Pipe Symmetry and its Applications in Symmetric and Antisymmetric Channel Flows," *J. Hydraul. Eng.*, vol. 146, no. 11, p. 06020014, Nov. 2020, doi: 10.1061/(ASCE)HY.1943-7900.0001813.

[16] N. Patel, J. Shahi, and J. Guo, "Applications of Second Log-Wake Law for Turbulent Velocity Distributions in Laboratory Flumes and Natural Rivers," *J. Hydraul. Eng.*, vol. 147, no. 9, p. 06021010, Sep. 2021, doi: 10.1061/(ASCE)HY.1943-7900.0001924.

[17] J. Guo, "The Log-Law of the Wall in the Overlap from a Functional Equation," *J. Eng. Mech.*, vol. 149, no. 2, p. 06022005, 2023.

[18] R. H. Karsten, J. M. McMillan, M. J. Lickley, and R. D. Haynes, "Assessment of tidal current energy in the Minas Passage, Bay of Fundy," *Proc. Inst. Mech. Eng. Part J. Power Energy*, vol. 222, no. 5, pp. 493–507, 2008.

[19] "FORCE." https://fundyforce.ca/ (accessed May 21, 2023).

[20] H. Viehman, D. Hasselman, T. Boucher, J. Douglas, and L. Bennett, "Integrating Hydroacoustic Approaches to Predict Fish Interactions with In-stream Tidal Turbines," *FORCE Rep.*, pp. 300–208, 2019.

[21] "Underway velocity measurements in the Alderney Race: towards a three-dimensional representation of tidal motions | Philosophical Transactions of the Royal Society A: Mathematical, Physical and Engineering Sciences." https://royalsocietypublishing.org/doi/full/10.1098/rsta.2019.0491 (accessed May 19, 2023).

[22] A. Naberezhnykh, D. Ingram, I. Ashton, and J. Culina, "How Applicable Are Turbulence Assumptions Used in the Tidal Energy Industry?," *Energies*, vol. 16, no. 4, Art. no. 4, Jan. 2023, doi: 10.3390/en16041881.

[23] D. Coles, "The law of the wake in the turbulent boundary layer," *J. Fluid Mech.*, vol. 1, no. 2, pp. 191–226, Jul. 1956, doi: 10.1017/S0022112056000135.

[24] J. McMillan, "Turbulence Measurements in a High Reynolds Number Tidal Channel," Jun. 2017, Accessed: May 21, 2023. [Online]. Available: https://DalSpace.library.dal.ca//handle/10222/72993